Supplementary Information

Modulating (001) plane growth in β-$Ni(OH)_2$ precursors: A pathway to controlling lithiation kinetics and enhancing the structural integrity of $LiNiO_2$

Chan Hwi Kim,[a,1] Yu Bin Choi,[a,1] Doo Seok Kwon,[a,1] JinHa Shim,[a] and Jin Ho Bang [a,b,*]

[a] Department of Applied Chemistry, Center for Bionano Intelligence Education and Research, Hanyang University ERICA, 55 Hanyangdaehak-ro, Sangnok-gu, Ansan, Gyeonggi-do 15588, Republic of Korea

[b] Department of Energy and Bio Sciences, Hanyang University ERICA, 55 Hanyangdaehak-ro, Sangnok-gu, Ansan, Gyeonggi-do 15588, Republic of Korea

AUTHOR INFORMATION

[1] These authors contributed equally to this work.

Corresponding author:

*jbang@hanyang.ac.kr

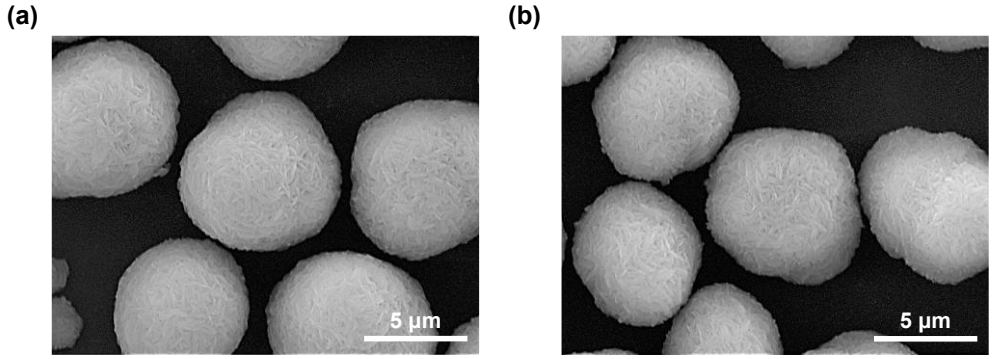

Fig. S1 SEM image of (a) L-Ni(OH)$_2$ and (b) H-Ni(OH)$_2$.

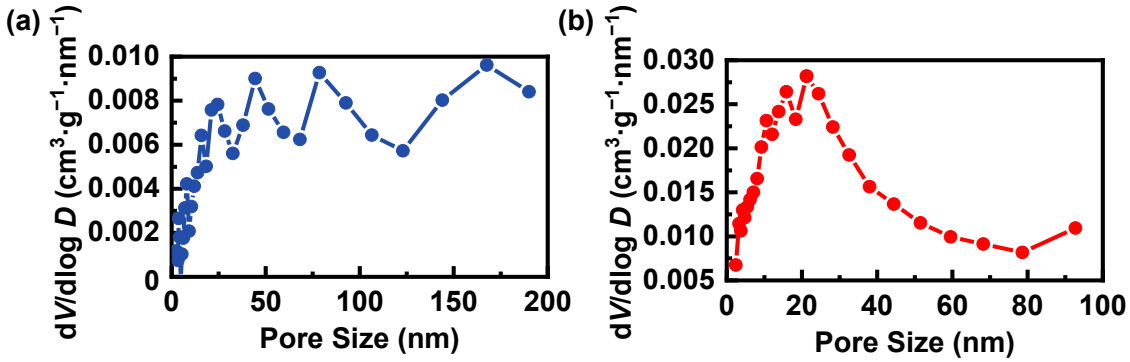

Fig. S2 Pore size distribution of (a) L-Ni(OH)$_2$ and (b) H-Ni(OH)$_2$, obtained using the BJH method.

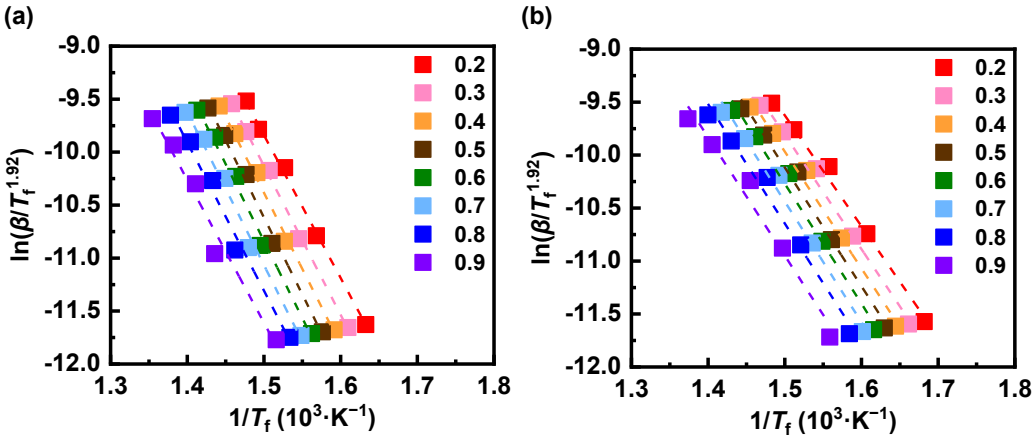

Fig. S3 Linear fitting results of $\ln(\beta/T_f^{1.92})$ versus $1/T_f$ for (a) L-LNO and (b) H-LNO.

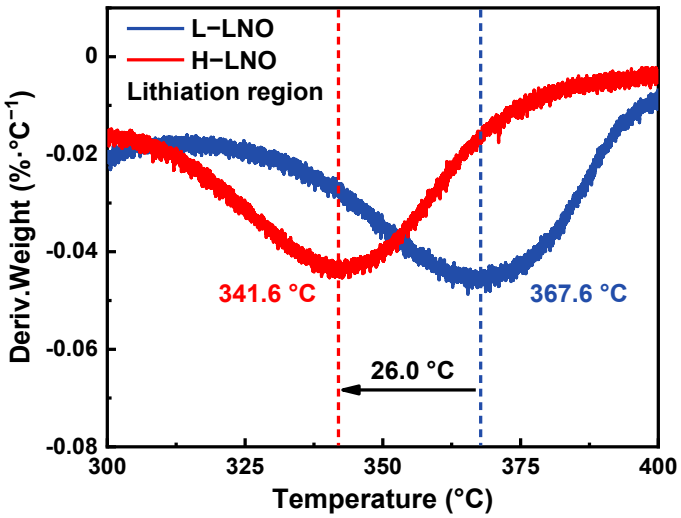

Fig. S4 Comparison of the derivative thermogravimetric curves of L-LNO and H-LNO in the lithiation temperature range. The data were recorded at a heating rate of 2 °°C min^{-1}, corresponding to the actual synthesis conditions.

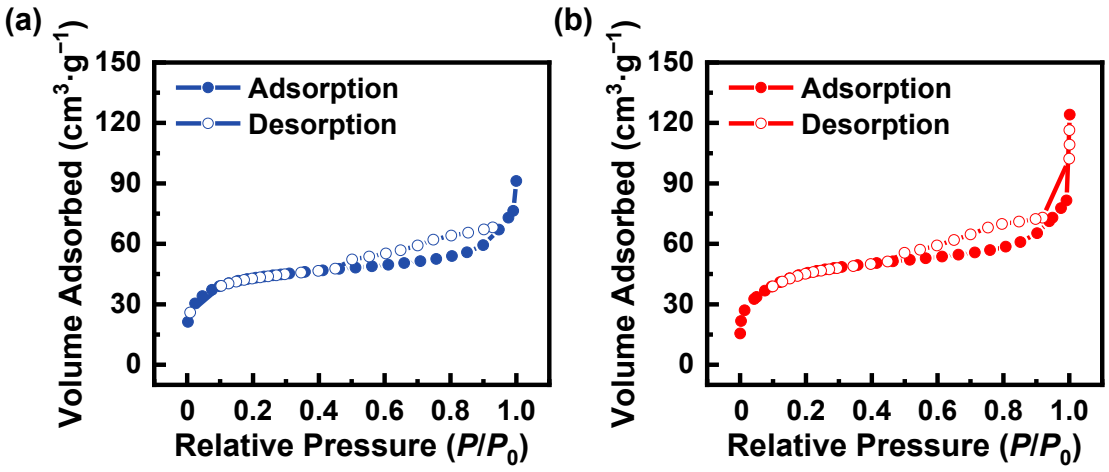

Fig. S5 N_2 adsorption/desorption isotherms of (a) L-$Ni(OH)_2$-derived NiO and (b) H-$Ni(OH)_2$-derived NiO after calcination at 300 °C.

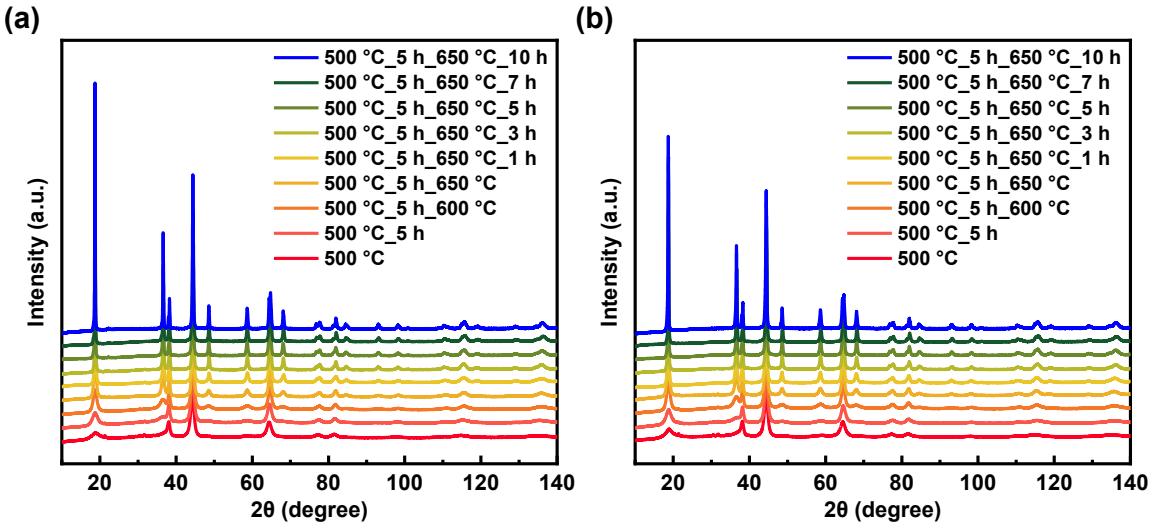

Fig. S6 Ex situ XRD patterns obtained during the calcination process of (a) L-LNO and (b) H-LNO.

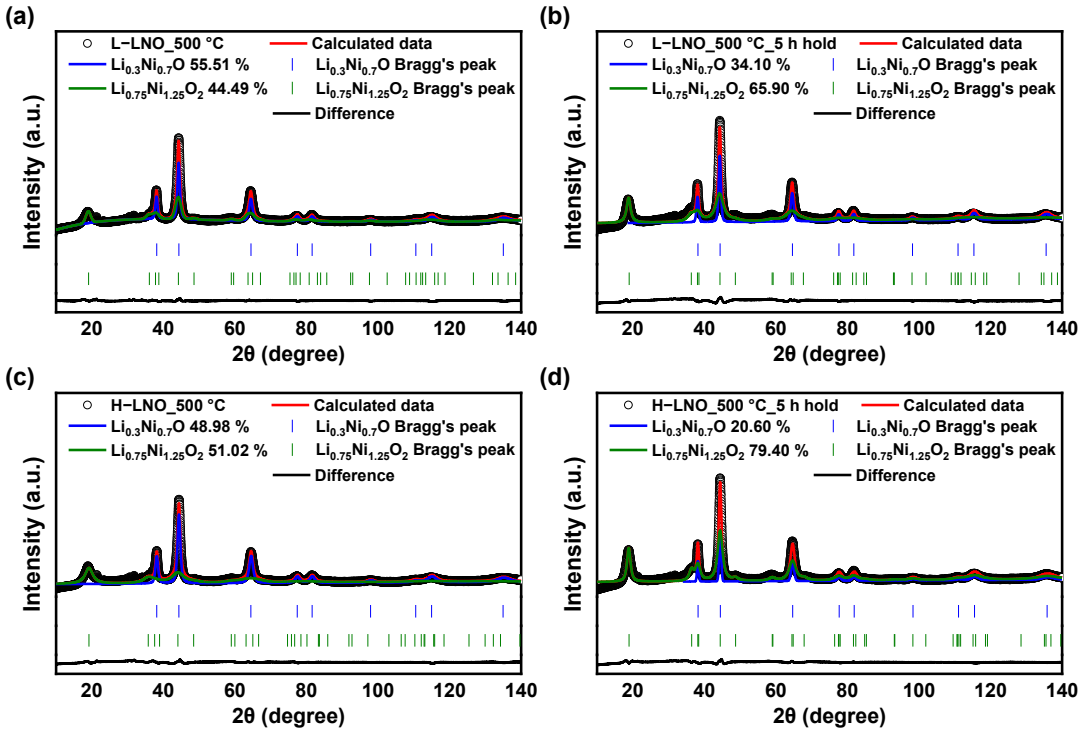

Fig. S7 Quantitative phase analysis by Rietveld refinement using XRD patterns collected during heating to 500 °C (Fig. S4a, S4b) and after 5 hours of isothermal holding at 500 °C (Fig. S4c, S4d) for L-LNO and H-LNO, respectively.

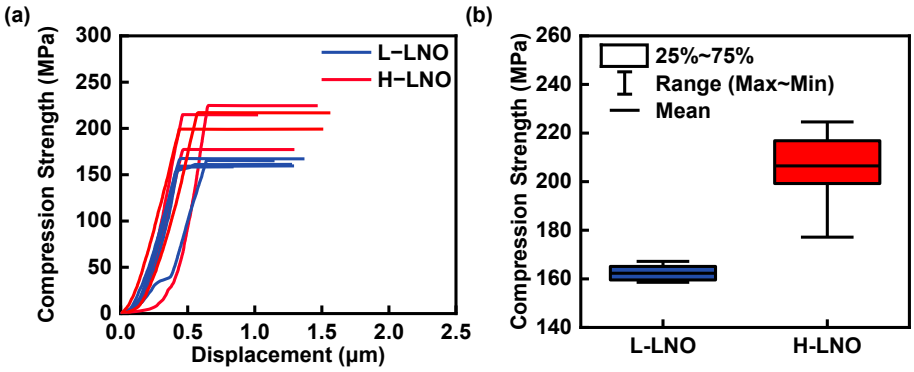

Fig. S8 (a) Representative micro-compression stress–displacement curves of L-LNO and H-LNO. (b) Box chart summarizing the compression strength of L-LNO and H-LNO. The box represents the interquartile range (25–75%), the whiskers indicate the maximum and minimum values, and the solid line denotes the mean value.

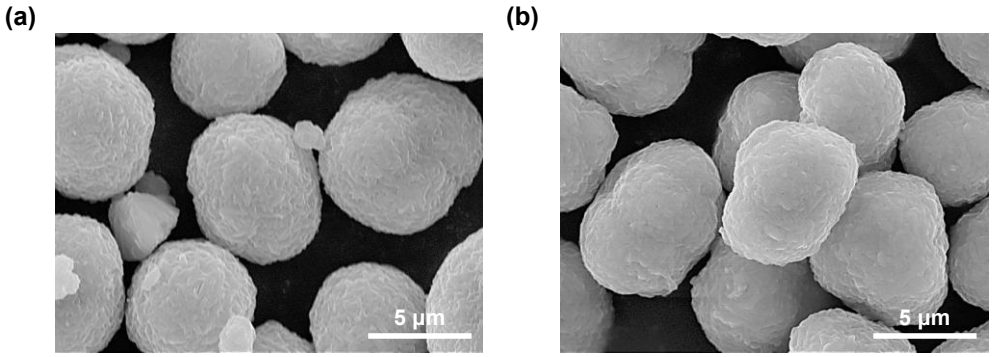

Fig. S9 SEM image of (a) L-LNO and (b) H-LNO.

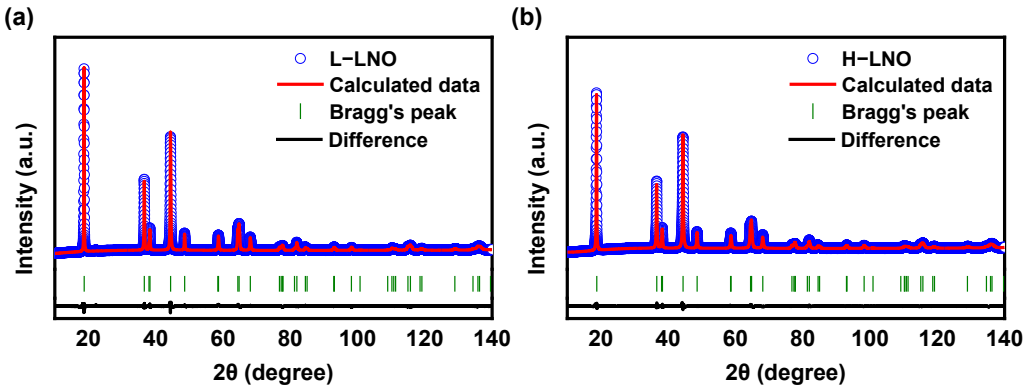

Fig. S10 Rietveld refinement results obtained from the XRD patterns of the final calcined (a) L-LNO and (b) H-LNO.

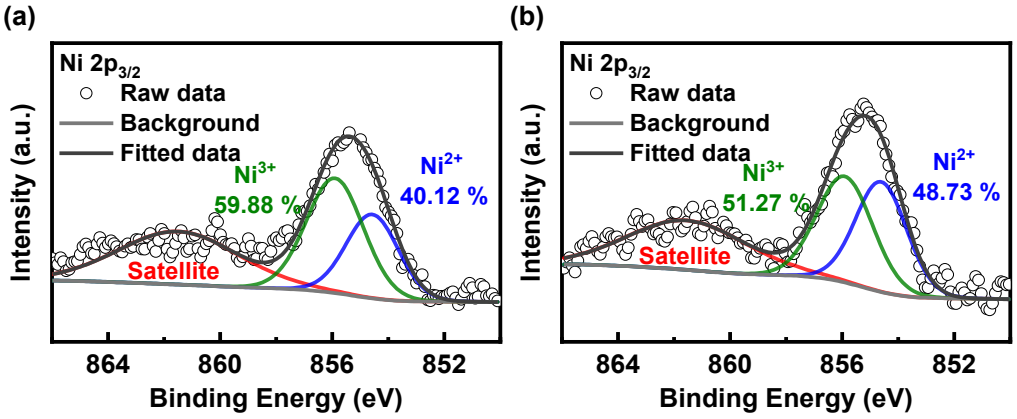

Fig. S11 Ni $2p_{3/2}$ XPS spectra of (a) L-LNO and (b) H-LNO.

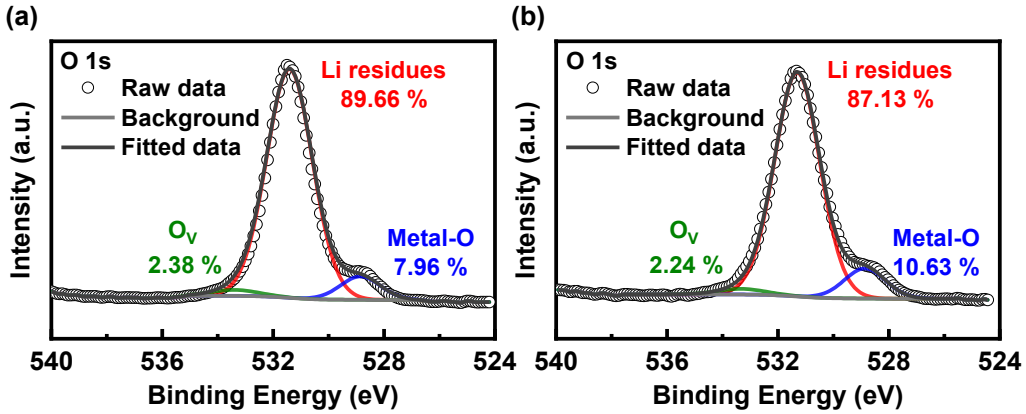

Fig. S12 O 1s XPS spectra of (a) L-LNO and (b) H-LNO, where O_v denotes oxygen vacancies.

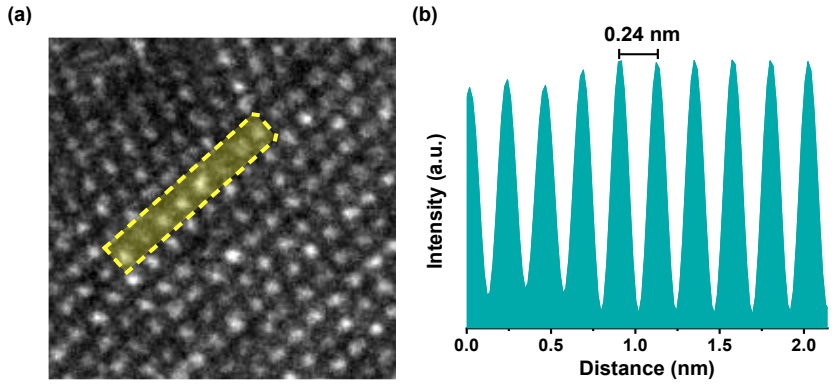

Fig. S13 (a) Inverse FFT image corresponding to Fig. 4e, and (b) the line profile obtained from the yellow dotted square region in (a).

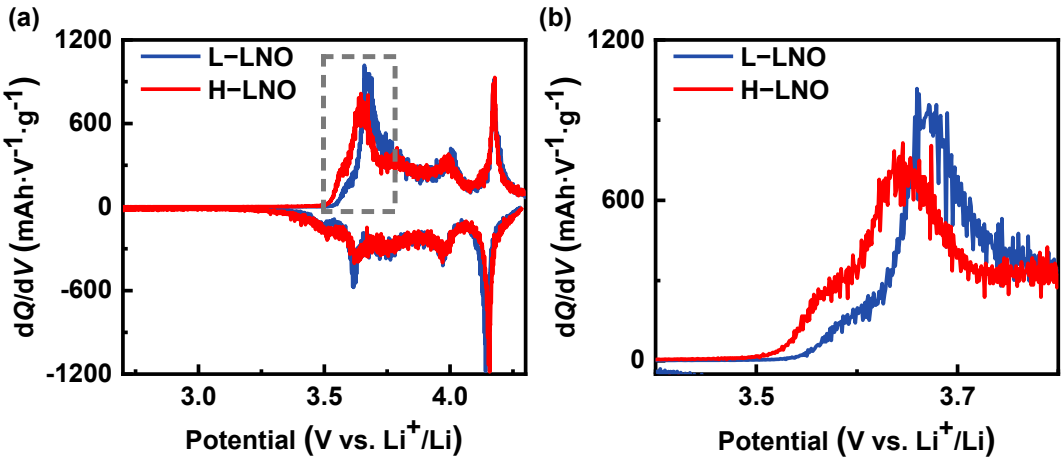

Fig. S14 (a) dQ/dV plots of the activation cycle for L-LNO and H-LNO, and (b) a magnified view of the initial oxidation region highlighted in (a).

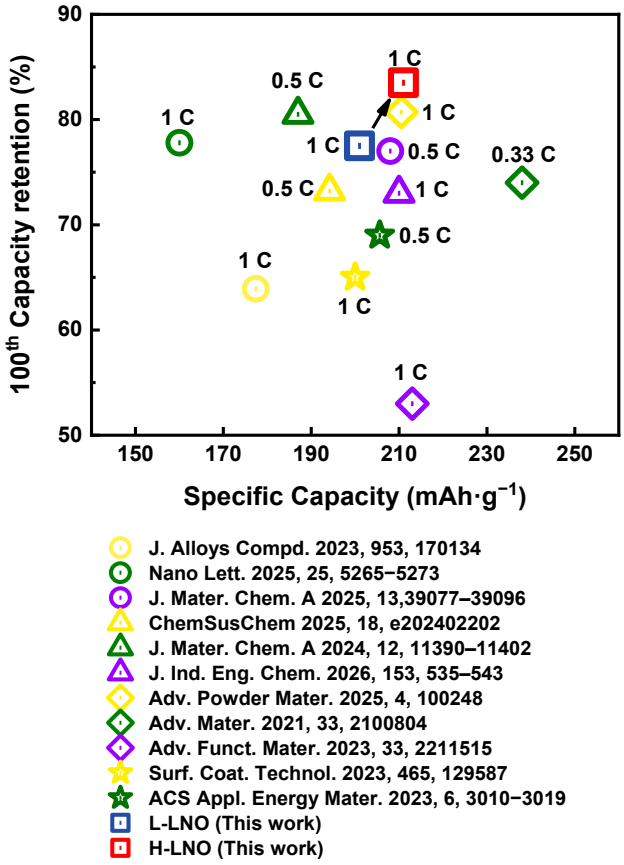

Fig. S15 Comparison of the electrochemical performance of L-LNO and H-LNO with previously reported LNO cathode materials from the literature.

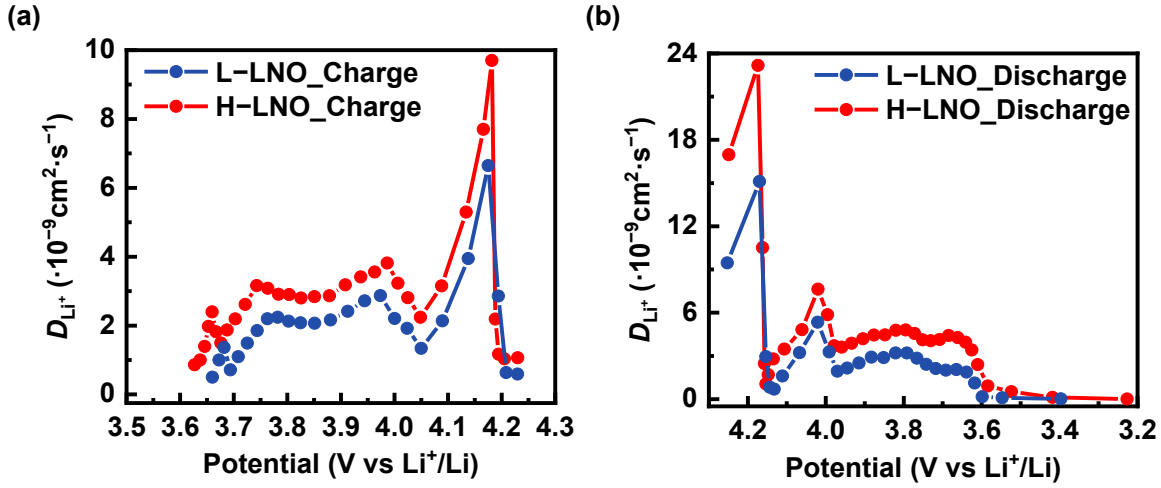

Fig. S16 Comparison of the Li^+ diffusion coefficients (D_{Li+}) of L-LNO and H-LNO during (a) the charging and (b) the discharging processes.

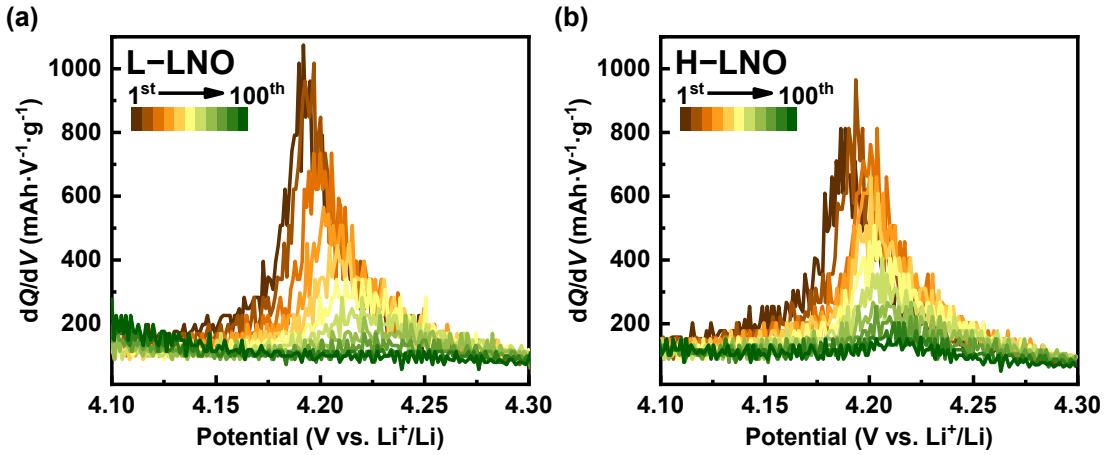

Fig. S17 Enlarged dQ/dV plots showing the H2 → H3 phase transition during 100 cycles for (a) L-LNO and (b) H-LNO.

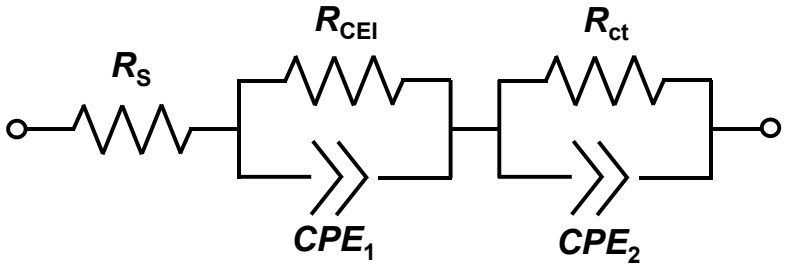

Fig. S18 Equivalent circuit model employed for the quantitative fitting of EIS data. The model comprises a series resistance (R_s) followed by two (R||CPE) elements connected in series: (R_{CEI}||CPE$_1$) representing the CEI resistance and (R_{ct}||CPE$_2$) representing the interfacial charge transfer resistance.